AL55 - A Study on Predicting Electrolyte Temperature of Aluminium Smelting Cells for Power Modulation

Choon-Jie Wong[1], Jie Bao[2], Maria Skyllas-Kazacos[3], Barry Welch[4], Jing Shi[5], Nadia Ahli[6], Amal Aljasmi[7], Mohamed Mahmoud[8] and Mustafa Mustafa[9]
1. Postdoctoral Research Fellow
2. Professor
3. Professor
4. Professor
University of New South Wales, Sydney, Australia
5. Lead Engineer, Research and Development
6. Manager, Technology Transfer Contracts
7. Area Engineer, Reduction Engineering
8. Manager, Centre of Excellence
9. Manager, Reduction Process and Lining Development
Technology Development and Transfer, Midstream
Emirates Global Aluminium (EGA), United Arab Emirates
Corresponding author: j.bao@unsw.edu.au

Abstract

The temperature and superheat of the electrolyte in the Hall-Héroult process play important role in achieving high energy and current efficiency. They provide the thermal energy to preheat materials, to allow phase changes of feeds and final product, and to complete the thermodynamic requirements (overall enthalpy of reaction). With the growing use of renewable energy sources that require frequent power modulation cycles, the monitoring and control of electrolyte temperature and superheat in real-time is becoming pivotal as power input is varied. However, this has been challenging because conventional thermocouples, and their protective sheaths, are rapidly corroded by the electrolyte and thus are unreliable for continuous operation. This paper reports the positive outcome for the continuous model-predictive monitoring of electrolyte temperature, even under power modulation conditions, by embedding thermocouples in the pot lining and on the pot shell for thermal balance calculations. This paper contributes to the monitoring of aluminium smelting cells, especially under variable power conditions, and provides valuable information for optimising cell operations and developing automatic process control systems.

Keywords: Bath temperature monitoring, Power modulation, Real-time monitoring, Model-based soft sensor, Aluminium reduction.

1. Introduction

Controlling both the operating temperature and the electrolyte composition within narrow bands is crucial for achieving high energy efficiency and long cell life of aluminium smelting cells. The electrolyte temperature and its superheat (the difference between bath and liquidus temperature) play important roles in achieving high current efficiencies through limiting the solubility of metal, in maintaining a protective frozen cryolitic ledge on the sidewall refractory, and in limiting the sidewall heat losses and thus the required energy for the process. The coupled variable, superheat, also needs to be always controlled within a narrow band because of the important role it plays in dissolving the batches of alumina that are added at a regular interval.

The process control tasks have always been challenging due to difficulties in process monitoring. Sensors, such as conventional thermocouples and their protective sheaths, are unreliable for

continuous operation because of their rapid corrosion by the electrolyte. However, proper process monitoring and control is achieving greater importance in the "renewable energy era" with intermittent energy supply sources requiring frequent power modulation, where cells must operate with varying power input to balance their loads on the power supply grid.

This paper reports the positive outcome for overcoming the challenge for continuous monitoring of electrolyte temperature under such circumstances, by embedding thermocouples in the pot lining and on the pot shell for thermal balance calculations. This methodology will be more reliable than data-based (artificial intelligence) or empirical model-based approaches [1-5], given the lack of high-quality power modulation data with good operation. The long-term aims are to ascertain whether such an approach opens the doors for better thermal control of operating cells when subject to power modulation, and to subsequently develop appropriate cell models and control strategies, including the monitoring and control of cell superheat.

2. Power Modulation

Early power modulation of aluminium smelting cells was considered for multiple reasons, such as mitigating high energy costs or addressing power supply deficiencies [6-9]. In many instances, operational difficulties and process control challenges were reported, including excessive cooling and ledge/freeze build-up [9-12]. Over recent decades, power modulation has regained importance due to the increasing use of intermittent renewables in our energy mix. Due to aluminium smelters being large energy users, they are commonly contractually obligated to provide demand-side response for power grid balancing, thus it becomes impractical to operate the cells continuously at fixed line current.

Renewable sources typically exhibit a diurnal cycle pattern, leading to power modulation schemes in which the power input is also cycled daily [13]. With such a frequency, it is impractical to balance the mass and heat transfers perfectly always. For example, the anode cover thickness of all cells in a potline cannot be altered twice daily to maintain heat loss when power, and consequently heat generation, are varied. Therefore, the control goal may shift, from maintaining a fixed range for electrolyte temperature and composition, to allowing these ranges to fluctuate with line current.

For example, as line current is varied, there is a limit on the amount of heat compensation achievable by adjusting cell voltage through anode-cathode distance (ACD). A low ACD value results in efficiency losses due to increased back reaction caused by the proximity of anodic gases and cathodic metal [12]. Conversely, a high ACD value could pull the anodes out of the electrolyte. For a modern cell technology considered in this paper, with a typical anode immersion depth of 15 cm, the anodes can only be elevated by a maximum of 1.3 cm. This is because electrolyte height is sensitive to anode immersion depth, as modern cells have high anodes-to-electrolyte volume ratio. Additionally, substantial anode beam movement can lead to crust breakage and materials falling into the electrolyte [14]. Other smelters have explored forced air cooling [15, 16] and shell heat exchanger [17] to increase heat removal rate during line current increase [18-22], but its impact on electrolyte temperature will be slow due to the large time constant introduced by the refractory insulators in the cell walls. This implies that under greater magnitudes of power modulation, the electrolyte temperature is expected to shift to a different range, hence it is increasingly crucial to continuously monitor and control it so it remains within acceptable bounds.

Similarly, under power modulation schemes, it is not necessary to control the concentration of alumina and other materials to the same level. Although the base-feeding rate of alumina must adapt to the line current because the current drives the rate of electrochemical reactions, the alumina concentration level can vary. For example, at a larger line current, the alumina

concentration level can be raised (up to certain limits), aiding mass transport to the electrode double layer due to a steeper concentration gradient. This also reduces the anodic overpotential which can limit the production of perfluorocarbon gases [23]. Alumina and other mass balances are mentioned here for completeness but will not be the focus of the remainder of this paper.

3. Thermocouples in Pot Lining and Shell

With smelting potlines having to operate on a diurnal cycle of power modulation, the opportunity was taken to install thermocouples in several EGA commercial cells. More than 40 thermocouples were embedded in different locations in the cell lining, and over 50 thermocouples were mounted along the length of the pot shell, providing a spatial temperature profile of each cell. This allows investigations into the potential of such measurements for better thermal monitoring and control when cells are subjected to power modulation, and subsequently develop appropriate cell thermal models.

Figure 1 illustrates the position of five of the thermocouples used in this study to predict the electrolyte temperature. These selected locations enable the monitoring of side and bottom heat losses, the variation in heat generation for the centre-channel zone where there exists additional thermal demand for alumina dissolution, and the potential effect of contact resistance changes. These thermocouples are also closest to the cell cavity, ensuring that the thermal resistance from the electrolyte to the sensors is minimal. This strategy reduces model-plant coefficient uncertainties and time lags in thermal transfer introduced by the refractory materials.

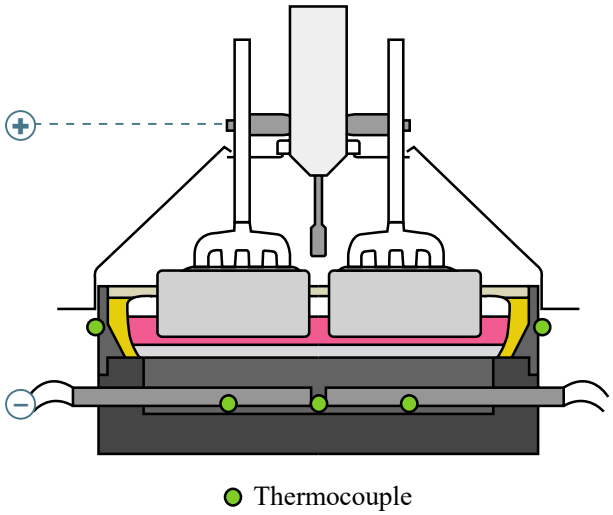

Figure 1. Locations of thermocouples for measurements used in this paper.

3.1 Data Processing for Usage as Model Input

The measurements from the high number of installed thermocouples still cannot fully represent the spatial variation that exists in a cell. Figure 2 shows one of 800 thermal images of the pot shell taken with Fluke Ti32 thermal imager; the pot shell exhibits spatial temperature variation and even contains a hot spot. The pot shell, in the absence of shell cooling fins, will be the hottest at the electrolyte-metal interface due to higher heat transfer coefficients [19] and the thinnest ledge resulting from turbulence induced by anodic gas bubble release and metal pad oscillations. Meanwhile, the pot shell temperature is lower at greater and lower vertical heights.

However, in a previous internal EGA study which measured the pot shell temperatures for over five months at five vertical heights on both sides of the shell, the vertical temperatures exhibited similar dynamics and their vertical temperature difference has remained quite consistent. This

means that while the localised temperature measurements will have offsets, the recorded dynamics is still representative of the much wider area of the pot shell.

Analyses of the captured thermal images, including that of Figure 2, show that the localised measurements at the thermocouple mounting locations (in between the fins) are on average approximately 50 °C lower than the mean pot shell temperature. This means that the localised pot shell temperature measurements require an offset 'calibration' to represent the dynamics of the larger area of the pot shell. Of course, this offset is valid only for the specific position of the mounted thermocouples. Similarly, the pot lining temperature measurements for the specific thermocouple positions were offset by +150 °C to obtain the average bottom lining temperature to be used in the model. These temperature series data can then be used as real-time inputs for the dynamic model described in the next section.

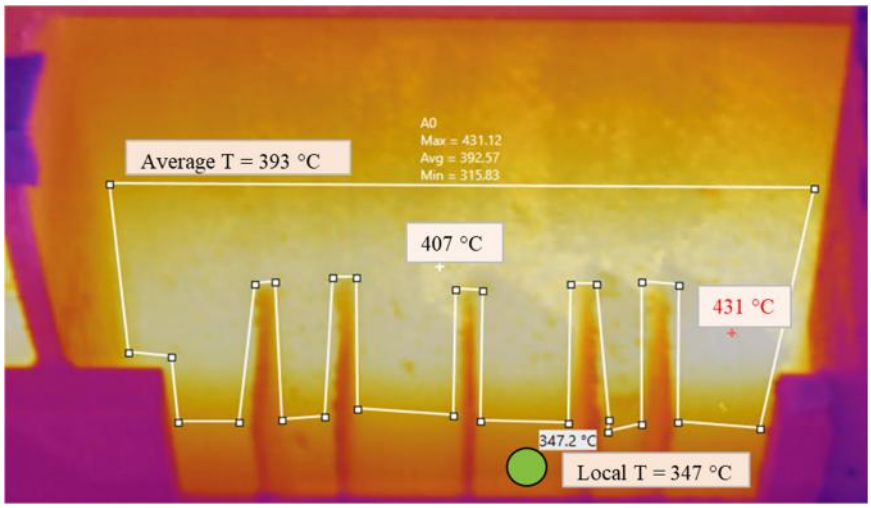

Figure 2. Pot shell exhibits spatial temperature variation; local thermocouple measurement is lower than the mean shell temperature at the liquid region.

4. Basis of Dynamic Model

For an accurate prediction of electrolyte temperature, simple correlations with the pot lining and shell temperatures will not suffice, because they still lag significantly behind the electrolyte temperature due to the low thermal conductivity of the materials. A simulation study conducted by Gusberti et al. [24] shows that following a step change in line current, the pot shell temperature typically takes at least 16 hours to stabilise at a new state. Hence, the electrolyte temperature dynamics must be computed with a dynamic model that performs a heat balance around the electrolyte and metal region of the cell. This approach is more reliable than data-based ones or those based on empirical relations, due to the lack of high-quality power modulation data with good operation.

The thermal balance is performed as follows: The readily available line current and cell voltage measurements are used to compute energy dissipation into the control volume ('generation'); the alumina feeding control action and line current are used to compute the process energy and other thermal requirements ('consumption'); the pot lining and shell temperatures allow calculation of heat losses from the bottom and sides of the cell ('output').

The energy dissipation at the electrode interface and the electrolyte region provides the rate-enabling electrochemical reaction energy for all reactions that occur at the electrode interfaces and all thermal energy requirements. The thermal energy requirements range from preheating and phase changes of all materials introduced to the cell, to the energy needed to convert the new

structural products to their final phase, to the heat loss through the pot shell and cover material. The energy dissipation is given by:

$$E_{\text{diss}} = IV - I^2 R_{\text{ext}} \tag{1}$$

where:

E_{diss} Energy dissipation rate, W
I Line current, A
V Cell voltage, V
R_{ext} Electrical resistances external to the control volume, Ω.

This electrochemical process requires energy to produce the product metal. As alumina feed (with impurities) is introduced, around 0.596 kWh/kg feed is required to preheat the material to operating temperature and to dissolve it. Energy is also required for preheating carbon anodes and other feeds, for phase changes of feeds and final product, and for enabling and completion of the electrochemical reactions. For a modern cell technology with a net anode carbon consumption of 0.40 kg C/kg Al and a gross of 0.50 kg C/kg Al, this requires around 5.474 kWh/kg Al [25-27]. With units treated carefully, the process energy is:

$$E_{proc} = \left(0.596\ \text{kWh/kg feed}\right) m_{\text{feed}} + \left(5.474\ \text{kWh/kg Al}\right) \frac{26.982\,\eta}{96\,485 \cdot 3} I \tag{2}$$

where:

E_{proc} Process energy rate, W
m_{feed} Total alumina mass fed in a minute, kg/h
η Current efficiency, fraction.

The heat loss to the ambient can be divided into three components: heat loss through the top, bottom, and sides of the cell, as illustrated in Figure 3.

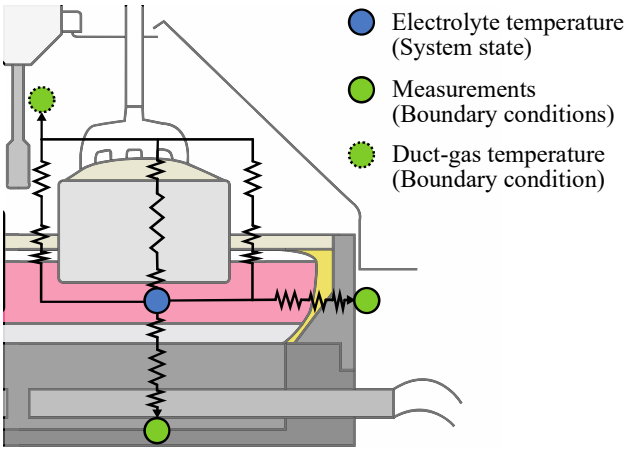

Figure 3. Simplified illustration of thermal transfers in the model.

The heat loss from the aluminium smelter cell can be represented with the following equation:

$$E_{\text{loss}} = \frac{T_{\text{B}} - T_{\text{gas}}}{R_{\text{B-gas}}} + \frac{T_{\text{B}} - T_{\text{lining}}}{R_{\text{B-lining}}} + \frac{T_{\text{B}} - T_{\text{shell}}}{R_{\text{B-shell}}} \tag{3}$$

where:

E_{loss} Heat loss rate to ambient, W
T_{B} Electrolyte (bath) temperature (metal temperature is assumed to be the same), K

T_{gas} Inside the hood gas temperature, K
T_{lining} Pot lining temperature (measured), K
T_{shell} Pot shell temperature (measured), K
$R_{\text{B-gas}}$ Thermal resistance between bath and chamber gas, K/W
$R_{\text{B-lining}}$ Thermal resistance between bath and pot lining, K/W
$R_{\text{B-shell}}$ Thermal resistance between bath and pot shell, K/W.

In the above equation, the heat flux equations are represented with equivalent thermal resistances for brevity. The relations for these thermal resistances have been published elsewhere [28-30]; they were calculated from the effective conductive heat transfer through each material and convective heat transfers through fluid solid interfaces. The top heat transfer includes heat losses through the anodes in contact with the electrolyte and the crust layer, as well as that through the air gap between the electrolyte and the crust. Meanwhile, the bottom and side thermal resistances are dependent on the thermal properties of the cell construction materials, as well as their thicknesses.

Finally, with the above energy components, the bulk electrolyte temperature can be computed by solving the following differential equation:

$$\frac{\mathrm{d}T_{\text{B}}}{\mathrm{d}t} = \frac{1}{m_{\text{B}}c_{\text{B}}}\left[E_{\text{diss}}(I,V) - E_{\text{loss}}\left(T_{\text{lining}}, T_{\text{shell}}, T_{\text{B}}\right) - E_{\text{proc}}(m_{\text{feed}}, I) \right] \quad (4)$$

where:
m_{B} Mass of electrolyte and metal, kg
c_{B} Weighted heat capacity of electrolyte and metal combined, J/K.

5. Results and Discussions

In this section, the electrolyte temperature is predicted using the dynamic model described in Section 4. This model uses the pot lining and shell thermocouple measurements described in Section 3 as boundary conditions for solving the state equation, Equation (4). Other model inputs are the line current, cell voltage, and alumina feeding control actions; these are conventional measurements/data readily available in all smelters.

5.1 Model Prediction During Power Modulation

The potline section, in which the cells are fitted with thermocouples, underwent a series of current reductions. At 8:07 am, the line current was reduced from 500 kA to 480 kA (a 4 % reduction) for 6 hours. Subsequently, it was further reduced to 475 kA (a total reduction of 5 %). The dynamic model was provided inputs for this period, and the predicted electrolyte temperature is plotted in Figure 4. For comparison, electrolyte temperatures from five locations, denoted in Figure 5, were also measured with Heraeus FiberLab and Marshall tip thermocouple at 30 minutes interval and plotted.

Figure 4 shows that the model predicted trend for electrolyte temperature reflects well that of the measurements. The predicted temperature up until 9:30 am was slightly higher than measured ones, due to the arbitrary choice of 960 °C (a typical cell operating temperature) as the initial condition for the dynamic model. From 9:30 am to 3:00 pm, the predicted temperature falls within the range of spatial temperature measurements. By analysing the dynamic model, Section 5.2 will show that the error due to arbitrary initial guess will be rejected over time.

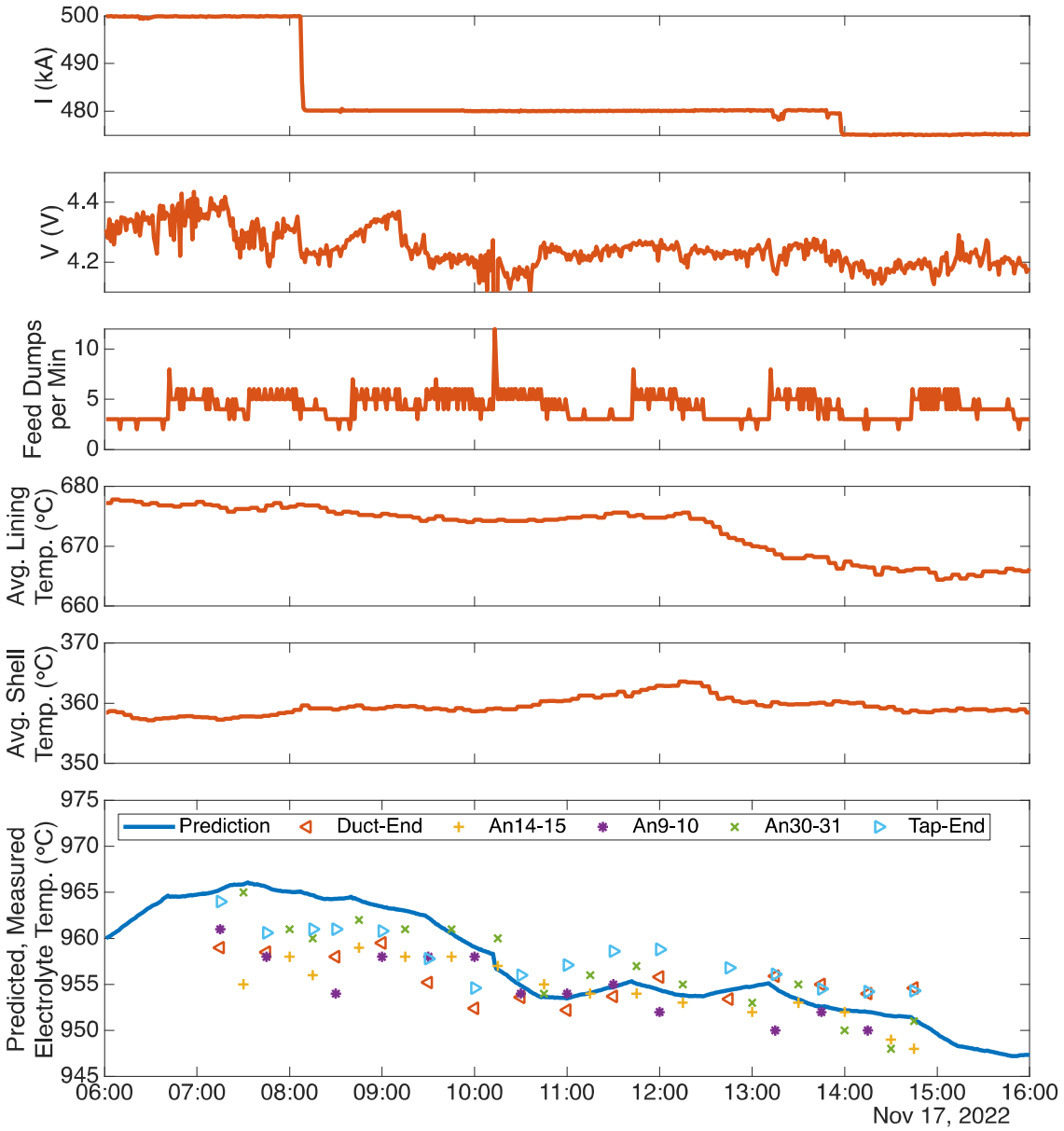

Figure 4. Model inputs and predicted/measured electrolyte temperatures during power modulation.

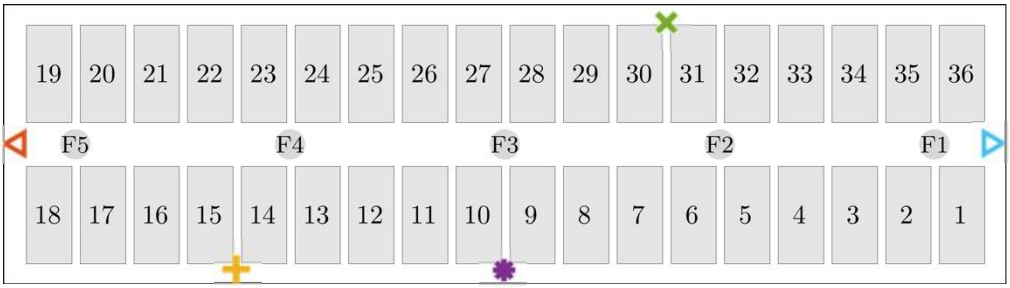

Figure 5. Location of electrolyte temperature measurements.

It can also be seen that following current reduction, the electrolyte temperature declined by about 15 °C during the measurement campaign, as the amount of joule heating has decreased. This was captured by the model prediction, which also includes fast dynamics arising from beam

movements and alumina feeding cycles. Additionally, Figure 4 also shows that there is no clear direct correlation between electrolyte temperature with both the pot lining and shell temperature measurements, due to the thermal insulations acting as low-pass filters that remove fast dynamics and introduce lags in the temperature response. This is why direct correlations of pot lining and shell temperatures to electrolyte temperature will not work, whereas by considering the energy balance, the proposed model-based approach works well.

5.2 Model Prediction Over 10 Days and Analysis of Model Stability

To demonstrate stability of the dynamic model over a longer period, the same model was provided over 10 days of the previously described model inputs. Figure 6 compares the prediction of the electrolyte temperature with the tap-end measurements that are recorded daily as part of standard operation. It also shows that the low frequency of daily tap-end measurements does not fully reveal the trend in electrolyte temperature.

Figure 6 Model inputs and predicted/measured electrolyte temperatures over 10 days.

The model output over time does not depend on the choice of initial conditions. This can be proven by rearranging Equation (4) to isolate the state T_{B}:

$$\frac{\mathrm{d}T_{\mathrm{B}}}{\mathrm{d}t} = -\frac{1}{m_{\mathrm{B}}c_{\mathrm{B}}}\left[\frac{1}{R_{\mathrm{B-gas}}}+\frac{1}{R_{\mathrm{B-lining}}}+\frac{1}{R_{\mathrm{B-shell}}}\right]T_{\mathrm{B}} + \mathrm{f}\left(I, V, T_{\mathrm{lining}}, T_{\mathrm{shell}}, m_{\mathrm{feed}}\right) \qquad (5)$$

where:

f Function representing the input terms (independent of the electrolyte temperature model variable, T_{B}). $I, V, T_{\mathrm{lining}}, T_{\mathrm{shell}}$ are measurements from the actual cell, and m_{feed} is known/recorded.

The model is stable if and only if the coefficient of the state is negative [31]. It is evident that this is true, since the control volume properties (m_{B}, c_{B}) and thermal resistances ($R_{\mathrm{B-gas}}$, $R_{\mathrm{B-lining}}$, $R_{\mathrm{B-shell}}$) are always positive. Therefore, the prediction error due to the arbitrary choice of initial condition will be rejected over time.

6. Conclusions

The monitoring and control of electrolyte temperature and its superheat are important to ensure high current efficiencies, to maintain desired ledge profile, and to limit heat losses. This study shows that a dynamic model can predict the bulk electrolyte temperature, even under power modulation conditions. This improves observability of the process, especially under non-standard operating conditions where power input is varied.

Measurements from thermocouples embedded in the pot lining and mounted on the shell of commercial cells were treated as boundary conditions for estimating bottom and side heat losses. By also calculating the process energy and the energy dissipated at the electrode interface and the electrolyte, it is possible to conduct a thermal balance around the electrolyte and metal region. The electrolyte temperature trends predicted by the model also reflects the fast dynamics of anode beam movements and alumina feeding cycles, which are not directly observable from the pot lining and shell temperature measurements. This paper has demonstrated that while pot lining and shell temperatures cannot directly indicate electrolyte temperature, they have potential in model-based approaches for thermal balance computations. Other model inputs required for this approach are line current, cell voltage, and alumina feeding control actions — all of which are readily available measurements/data.

While these findings are encouraging, more robust methods can be developed for real-time soft sensor implementations. For example, it can be automatically calibrated as new daily temperature measurements are conducted. Future work also includes expanding this paper to monitor the spatial electrolyte temperature and superheat, similar to the discretisation level achieved in other works [29, 30, 32-34]. This also requires freeze dynamics to be included, which will couple the mass and thermal balance via phase changes of the ledge. This is becoming important as larger cells are being built and operated at higher amperages. This will provide valuable spatial process information for optimising cell operations and developing automatic process control systems, leading to improved energy efficiency and lowered operational costs under power modulation schemes. More technical and economic analysis should also be conducted to optimise the quantity and the placement of thermocouples to increase sensor life and reduce capital cost.

7. References

1. Fred Frost and Vishi Karri, Productivity improvements through prediction of electrolyte temperature in aluminium reduction cell using BP neural network, *PRICAI 2000 Topics in Artificial Intelligence: 6th Pacific Rim International Conference on Artificial Intelligence*, Melbourne, Australia, 2000, 490-499.
2. Fábio M. Soares and Roberto C. L. Oliveira, Modelling of temperature in the aluminium smelting process using Neural Networks, *Proceedings of the International Joint Conference on Neural Networks (IJCNN)*, 2010, 1-7.
3. Alan Marcel Fernandes de Souza et al., Soft sensors in the primary aluminum production process based on neural networks using clustering methods, *Sensors*, Vol. 19, No. 23, (2019), 5255.
4. Najeeba Aljabri et al., Advanced process control with smart smelter sensors at EGA, *Proceedings of the 40th International ICSOBA Conference*, Athens, Greece, 10-14 October 2022, Paper AL05, *Travaux* 50, 1049-1060.

5. S. Kolås and T. Støre, Bath temperature and AlF_3 control of an aluminium electrolysis cell, *Control Engineering Practice*, Vol. 17, No. 9, (2009), 1035-1043.
6. Hánderson Penna Dias, Brazil 2001 Energy Crisis -- The Albras Approach, *Light Metals* 2004, 707-711.
7. Jean Yamamoto, Leonardo Paulino, and Carlos Eduardo Zangiacomi, Experiences with long power interruption periods and lower amperage operation in a VS Soderberg potline, *Light Metals* 2006, 427-432.
8. Willy Kristian Rolland et al., Experience with power saving in the Soderberg lines at Hydro Aluminium Karmøy, *Light Metals* 2004, 179-184.
9. Till Reek, New approaches to power modulation at TRIMET Hamburg, *Light Metals* 2011, 375-379.
10. A. C. Brant Filho et al., The operation of a smelter with power modulation, *Light Metals* 1992, 357-362.
11. Pinheiro Leal J. Nunes, A. Vianna da Silva, and L.F. Gomes Soutinho, Power modulation on Valesul P-19 pots, *Light Metals*, 1998, 1267-1272.
12. Till Reek, *Power Modulation of aluminium Reduction Cells -- Operational Constraints and Process Limits*, Ph.D. thesis, School of Chemical Engineering, Faculty of Engineering, the University of New South Wales, Australia, 2015.
13. Marco A. Stam and J. Schaafsma, The impact of power modulation on the cell dynamics, *Proceedings of 9th Australasian Aluminium Smelting Technology Conference*, Terrigal, Australia, 4-9 November 2007, Paper 47, 465-472.
14. Pierre-Yves Geay, Barry J. Welch, and Pierre Homsi, Sludge in operating aluminium smelting cell, *Light Metals* 2001, 222-228.
15. S. Guérard, Modelling and design of a forced convection network for Hall-Heroult cells, *Proceedings of the 34th International ICSOBA Conference*, Quebec, Canada, 3-6 October 2016, Paper AL09, *Travaux* 45, 571-578.
16. Jules Côté et al., Developing and implementing an efficient forced cooling network at Aluminerie Alouette, *Light Metals* 2022, 423-431.
17. Mark P. Taylor et al., Heat exchanger, filed November 2005.
18. Rio Tinto, Liberty Aluminium Dunkerque, 2019, https://www.ap-technology.com/wp-content/uploads/2019/03/AP_newsletter_2019_vfinale.pdf (Accessed on 1 March 2019).
19. Abdulla Habib Ahmed, *Manipulation of heat dissipation from sides of electrolytic cells*, Ph.D. thesis, School of Chemical Engineering, Faculty of Engineering, the University of New South Wales, Australia, 2015.
20. Pascal Lavoie et al., Increasing the power modulation window of aluminium smelter pots with shell heat exchanger technology, *Light Metals* 2011, 369-374.
21. N. Depree et al., The 'Virtual Battery' -- operating an aluminium smelter with flexible energy input, *Light Metals* 2016, 571-576.
22. Nick B. Depree, David P. Thomas, and David S. Wong, The contribution and economics of demand side response towards decarbonizing the aluminium smelting industry, *Light Metals* 2022, 560-570.
23. David Wong et al., Latest progress in IPCC methodology for estimating the extend of PFC greenhouse gases co-evolved in the aluminium reduction cells and challenges in reducing these emissions, *Proceedings of the 37th International ICSOBA Conference*, Krasnoyarsk, Russia, 2019, *Travaux* 48, 735-758.
24. Vanderlei Gusberti, *Modelling the mass and energy balance of aluminium reduction cells*, Ph.D. thesis, School of Chemical Engineering, Faculty of Engineering, the University of New South Wales, Australia, 2014.
25. Choon-Jie Wong et al., Studies on power modulation of aluminum smelting cells based on a discretized mass and thermal dynamic model, *Metallurgical and Materials Transactions B*, Vol. 54, (2023), 1-16.
26. Barry J. Welch, Training the trainers Part 1: Review of objectives constraints & changes, 2021.

27. Outotec, HSC Chemistry 5, 2002, https://www.mogroup.com/portfolio/hsc-chemistry/.
28. Choon-Jie Wong et al., Monitoring cell conditions and anode freeze dissolution with model-based soft sensor after anode change, *Light Metals* 2023, 87-94.
29. Choon-Jie Wong, *Dynamic mass and heat balance model of hall-heroult cells: A discretised approach*, Ph.D. Thesis, School of Chemical Engineering, Faculty of Engineering, University of New South Wales, Australia, 2022.
30. Choon-Jie Wong et al., Modelling of coupled mass and thermal balances in Hall-Heroult cells during anode change, *Journal of the Electrochemical Society*, Vol. 168, No. 21, (2021), 123506.
31. Dale E. Seborg et al., *Process dynamics and control*. 3 Edition, John Wiley & Sons, 2016.
32. Choon-Jie Wong et al., Discretized thermal model of Hall-Heroult cells for monitoring and control, *IFAC-PapersOnLine*, Vol. 54, No. 11, (2021), 67-72.
33. L. Tikasz, R. T. Bui, and V. Potocnik, Aluminium electrolytic cells: A computer simulator for training and supervision, *Engineering with Computers*, Vol. 10, No. 1, (1994), 12-21.
34. V. Potočnik et al., Aluminium electrolysis cell simulators as assistance tools for cell operation and control, *Proceedings of the 11th International Symposium of ICSOBA*, Balatonfüred, Hungary, 1996, *Travaux 23*, 267-283.